COBEM 2023 27TH INTERNATIONAL CONGRESS OF MECHANICAL ENGENEERING

ABCM Brazilian Society of Mechanical Sciences and Engineering
27th ABCM International Congress of Mechanical Engineering
December 04-08, 2023, Florianópolis-SC, Brazil

COB-2023-0970
A MODEL TO IMPROVE THE CONTROL OF THE LIQUID INJECTION VELOCITY IN A LAZY-WAVE RISER

Gabriela Pereira Toledo
Matheus Alexandre Pasquini
Jéssica Leonel Gonçalves
Ricardo Augusto Mazza
Flow&Rs Laboratory - School of Mechanical Engineering - Universidade Estadual de Campinas (UNICAMP), Rua Mendeleyev 200, 13083-860, Campinas, SP, Brazil
g235585@dac.unicamp.br
pmatheus@unicamp.br
jessicalg@cepetro.unicamp.br
mazza@unicamp.br

Abstract. *Engineers have been sizing single-phase hydraulic systems forever, and using system hydraulic curves to properly size the pump and valves to attend to the system requirements is a part of this process. In addition, these curves can be used as a method to control the system, especially for two-phase flow. When the gas enters the system, the operational condition changes. In this way, the pump rotation and valve opening must change to ensure operational conditions. These changes are corrected manually when the gas enters the test section. The present work aims to determine a methodology to automatically determine the pump rotational speed and flow control valve aperture to attend to the required water flow rate. The methodology can be used as a control procedure incorporated into supervisory systems. Making precise and fast air and water injection control on a complex test section is challenging. Due to the air compressibility, the bubbles expand as they rise in the test section. In addition to causing variations in air and water superficial velocities, this phenomenon causes the water column to lose weight, interfering with air and water injection velocities. The water injection control system uses a numerical model to estimate the two-phase flow pressure drop in the test section and the pump head curve. The numerical data is compared with an experimental two-phase air-water flow data set. Moreover, an experimental database for single-phase flow is used to adjust the valve flow coefficient CV and the pump's head curve CH. The system under analysis corresponds to an experimental lazy-wave riser apparatus from the Flow&Rs Lab. This apparatus has a diameter of 23.4 mm ID, a total dimensionless length of 2,142D, and a dimensionless height of 1,529D. Combining the pump head curve with the system flow coefficient makes it possible to predict the operational point in the intersections of the curves. The proposed model can predict the injection pressure of a two-phase flow with less than 15% deviation and the liquid superficial velocity with less than 20% deviation for all cases tested.*

Keywords: *hydraulic system, control method, lazy-wave riser, superficial velocities, two-phase flow*

1. INTRODUCTION

The two-phase flow occurs in many industrial sectors, such as nuclear reactors, petroleum extraction from wells, refrigeration systems in power plants, and other applications (Shoham, 2006; Bertola, 2014). Due to the two-phase flow widespread occurrence, the studies on this topic have increased in the last years (Kanizawa and Ribatski, 2021). Thus, the researchers reproduce the challenging industrial situations on a reduced scale to study the two-phase flow phenomena. Also, they must control the experimental conditions to set up the experimental point they need to study and to ensure each test's repeatability.

Therefore, it is desired that the experimental test section counts with a control system to manage the flow variables during the flow process, including the setup of the gas and liquid injection velocities. Many phase flow rate measurement techniques are available in the literature, as presented by Yan *et al.* (2018); Bahrami *et al.* (2019); Wang *et al.* (2020). However, there is a lack of studies on controlling the phase injection in two-phase flows.

Usually, this control is made employing a PID controller. However, this controller has some relevant limitations to fluid flow control. The PID controller adjusts the interest variables by inputting a correction factor that must be established for each process. That can be a time-consuming task. In addition, the PID controller did not present good results when controlling non-linear systems, as in the case of fluid flow (Wajman, 2019). Also, a single PID controller cannot control two components. Thus, when managing multiple components, multiple PID controllers are required. Due to its limitations, controllers based on fuzzy logic and neural networks have been used lately for fluid control (Ferraz *et al.*, 2022; Malhotra and Sodhi, 2011; Wajman, 2019). However, these controllers based on artificial intelligence need a model to determine

the system's flow conditions.

This paper is motivated by the lack of a model to improve the injection of liquid velocity to use in a controller. Therefore, given a gas mass flow rate, we aim to obtain a model to determine the pump rotation and the valve opening to achieve the desired liquid's superficial velocity. Defining these two variables for single-phase flow using the pump and systems head curves is common in the fluid flow field. However, when gas enters the test section, the water column loses weight, changing the system head curve and demanding a model to determine this new condition. This situation is even more challenging in a complex test section as a lazy-wave riser because of the inclination change and the gas expansion as the gas bubbles rise in the test section.

The model is based on the homogeneous model to estimate the two-phase pressure drop along the riser and determine the system flow curve. The injection pressure predicted numerically is compared with an experimental database of a lazy-wave riser of 23.4 mm ID, dimensionless length of 2,142D, and dimensionless height of 1,529D scaled by a real lazy-wave riser of the pre-salt to assess the model's capabilities. In addition, the experimental liquid superficial velocity obtained by inputting the predicted pump rotation and the valve opening is compared with the desired liquid's superficial velocity.

This paper is organized as follows: Section 2 describes the experimental apparatus; Section 3 presents the method and the mathematical model adopted; Section 4 presents the results and discussion of the study. Finally, Section 5 shows the conclusions.

2. EXPERIMENTAL SETUP

An experimental apparatus was assembled in the Flow&Rs Lab. for lazy-wave risers (SLWR) studies. Lazy-wave risers are found in several pre-salt oil fields to reduce mechanical efforts in this structure due to the water depth. A real pre-salt lazy-wave riser scaled the lazy-wave experimental apparatus. The experimental setup counts with air and water loops, ten instrumentation stations (S0 to S9) equipped with pressure transducers, an air compressor, a water pump, and a flow measurement station for each fluid, as shown in Fig. 1.

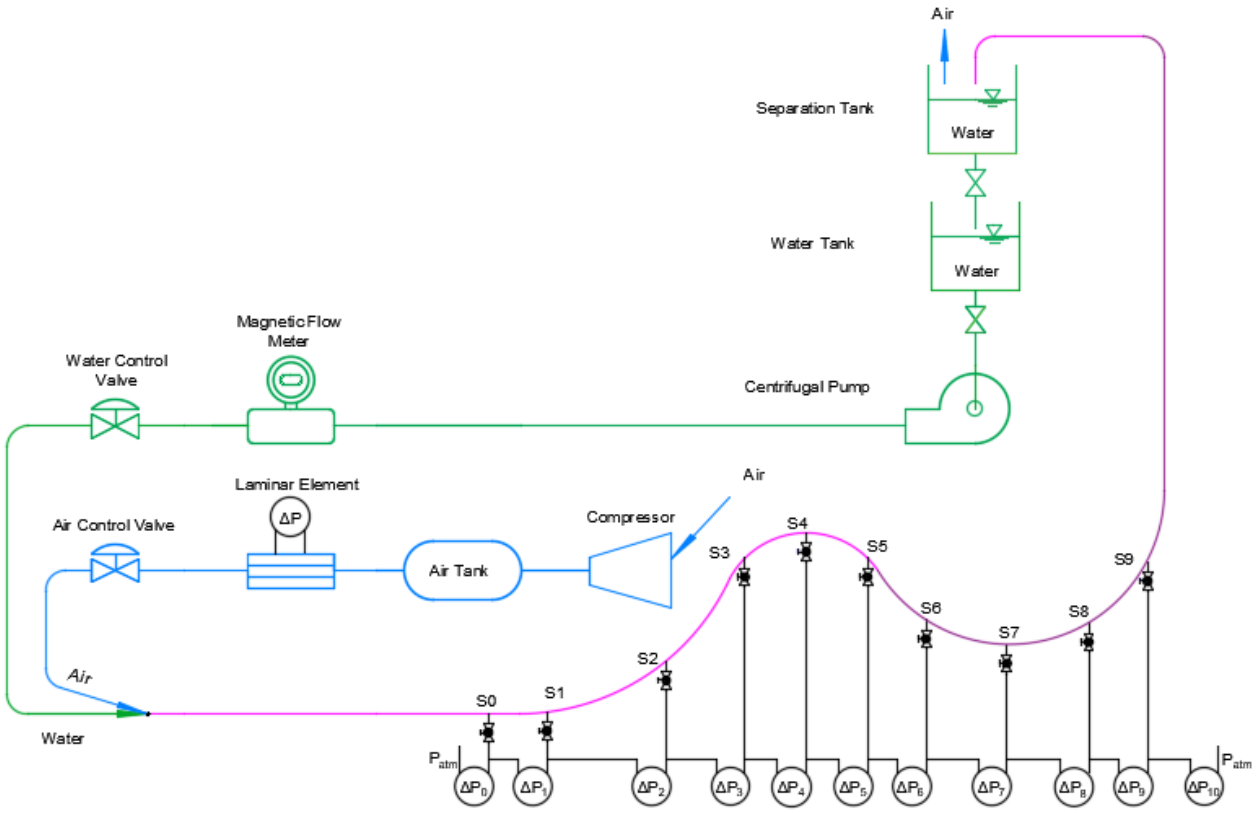

Figure 1. Schematic of the experimental test section; water loop (—), air loop (—) , and two-phase section (—).

The test section's schematic represents the lazy-wave riser's experimental apparatus. Figure 2 shows this experimental test section. This figure shows the horizontal part and the 'S' curve of the lazy-wave, where the measurement stations are positioned. After this section, the flowline connects in the vertical section, as represented in Figure 1.

In addition, Tab. 1 shows the range and accuracy of all instruments. The experimental apparatus is controlled using a

Figure 2. Lazy-wave experimental test section.

SCADA (Supervisory Control and Data Acquisition) running at the HiTecnologia PLC system. A LabVIEW supervisory system allows a graphical interface to easily operate and control the apparatus. The lazy-wave test section is instrumented with pressure transducers, and all data are sampled at 3 kHz using a National DAQ system model NI CDAQ-9188 and NI C9203 16 bits analogic input module.

Table 1. Range and accuracy of the equipment.

Equipment	**Localization**	**Range**	**Accuracy**
Rosemount 8750W	Waterline	$3x10^{-4}$ to $3.1x10^{-3}$ [m^3/s]	0.25% of the rate
Omega FMA-1609A-I2	Airline	0.02 to 3.55 [kg/h]	$\pm$ (0.8% of rdg + 0.2% of FS)
Meriam LFE 50MJ10-9	Airline	$2.25x10^{-4}$ to $1.59x10^{-3}$ [m^3/s]	0.8% of rdg
Rosemount 2051-CD4	Test section	-600 to 600 [kPa]	0.1% of the span
Rosemount 2051-CD1	Test section	-5.884 to 5.884 [kPa]	0.065% of the span
Rosemount 3051	Test section	-62 to 62 [kPa]	0.04% of the span
ZÜRICH Z.10		0 to 101.3 [kPa]	0.1% of the span

The air and water loops are supplied by a screw compressor and a centrifugal pump, respectively. The water flow rate is measured by a Rosemount electromagnetic flow meter model 8750W and is controlled by a frequency inverter WEG CFW-50 and a Fisher Baumann pneumatic globe valve model 24000CVF. The air mass flow rate is measured by an Omega laminar flow element (LFE) model FMA-1609A-I2 or Meriam LFE 50MJ10-9 plus Rosemount 2051 CD1 pressure sensor. The air mass flow rate is controlled manually using a JELPC mechanical air pressure regulator model BRF 4000 and a needle valve Swagelok. For our proposed study, it is assumed that we can control the air mass flow rate easily. The pressure transducers are differential, and the atmospheric pressure is measured by a barometer ZÜRICH Z.10.

The test section is a stainless steel OD tube with 23.4 mm ID and 50.13 m (2,142D) long that extends from the ground to 1,529D height. Ten measurement stations are positioned along the lazy-wave riser 6.44 m (275D), 7.56 m (323D), 9.25 m (395D), 10.94 m (467D), 11.81 m (505D), 12.69 m (542D), 13.79 m (589D), 14.90 m (637D), 16.00 m (684D), and 17.11 m (731D) from the injector. All ten stations have pressure transducers and dual impedance probes. The first

station (S0) is equipped with two pressure transducers; one measures the absolute pressure at the first station (P_0), and the other measures the pressure difference between this station and the following (ΔP_1). The pressure transducer in S0 is the Rosemount 2051 CD1 for the differential pressure and CD4 for the absolute pressure. The tenth station (S9) is also equipped with a Rosemount 2051-CD4 to measure the absolute pressure at this station. The other pressure transducers measure the pressure drop between two consecutive stations using the Rosemount 3051 pressure transducers. The pressure drop in the distance between the injector and S0 is mainly frictional. Thus, the pressure in these two points is almost the same; therefore, we assumed that the pressure at S0 is equal to the injection pressure P_{inj}.

Two PPR pipes compose the water loop, one of 1" and the other of 1.25". In addition to the pressure loss caused by the water pump and the control valve, other elements contribute to the minor pressure loss: tee junctions, y-tee junctions, elbows, flanges, contractions and expansions, and valves. Table 2 presents the minor head loss elements and the number of them for each pipe.

Table 2. Minor head loss elements.

Element	PPR 1"	PPR 1.25"	Stainless steel
Tee junction	4	7	3
Y-Tee junction	0	0	3
Elbow	7	10	0
Union/flange	9	9	15
Ball valve	4	0	3
Pneumatic valve	0	3	4
Contraction/expansion	3	0	0

3. MATHEMATICAL MODEL

The proposed model in this article aims to obtain the pump rotation and the control valve opening from a given desired gas and liquid superficial velocities. We need to obtain the system flow coefficient CH for our experimental setup to achieve this objective. This approach is well-known for single-phase flow; however, this task is a bit more challenging for two-phase flows. Nonetheless, the modeling of this system can be simplified, as shown in Fig. 3. In addition, Fig. 3 presents the sum of loss coefficients and equivalent lengths of the minor head losses, and the height of the water and two-phase sections.

In this approach, the system has two parts: the water and two-phase sections. The atmospheric pressure (P_{atm}) and the pressure at the injection point of the two-phase test section (P_{inj}) are the boundary conditions. The green line represents the single-phase part flowing water, the blue arrow represents the air entrance, and the magenta line represents the two-phase column. This two-phase column determines the injection pressure as given by Eq. (1).

$$P_{inj} = P_{atm} + \Delta H \left(\frac{dP}{dz}\right)_{hydrostatic} + \Delta L \left(\frac{dP}{dz}\right)_{frictional}, \tag{1}$$

where (dP/dz) is the pressure gradient, ΔH is the test section's vertical height, and ΔL is the total length.

The hydrostatic and frictional pressure gradients can be determined using a two-phase flow model. The mixture models are the most known two-phase models. They allow us to predict the flow parameters with reasonable accuracy, assuming the two-phase flow as a pseudo-fluid with properties given by the weighted average of each fluid. These models are well described in Wallis (2020). The mixture models encompass the homogeneous and the drift-flux models. They are essentially the same model; however, the homogeneous model supposes no-slip condition between the phases. Therefore, Eqs. (2) and (3) give the hydrostatic and frictional pressure drop parcels.

$$\left(\frac{dP}{dz}\right)_{hydrostatic} = \rho_M g, \tag{2}$$

$$\left(\frac{dP}{dz}\right)_{frictional} = 2C_f \rho_M \frac{J^2}{D}, \tag{3}$$

where g is the acceleration due to gravity, J is the mixture velocity, and D is the pipe inner diameter of the test section. ρ_M is the mixture density, and C_f is the Fanning's frictional factor, given by Eqs. (4) and (5), respectively:

$$\rho_M = \alpha\rho_G + (1-\alpha)\rho_L, \tag{4}$$

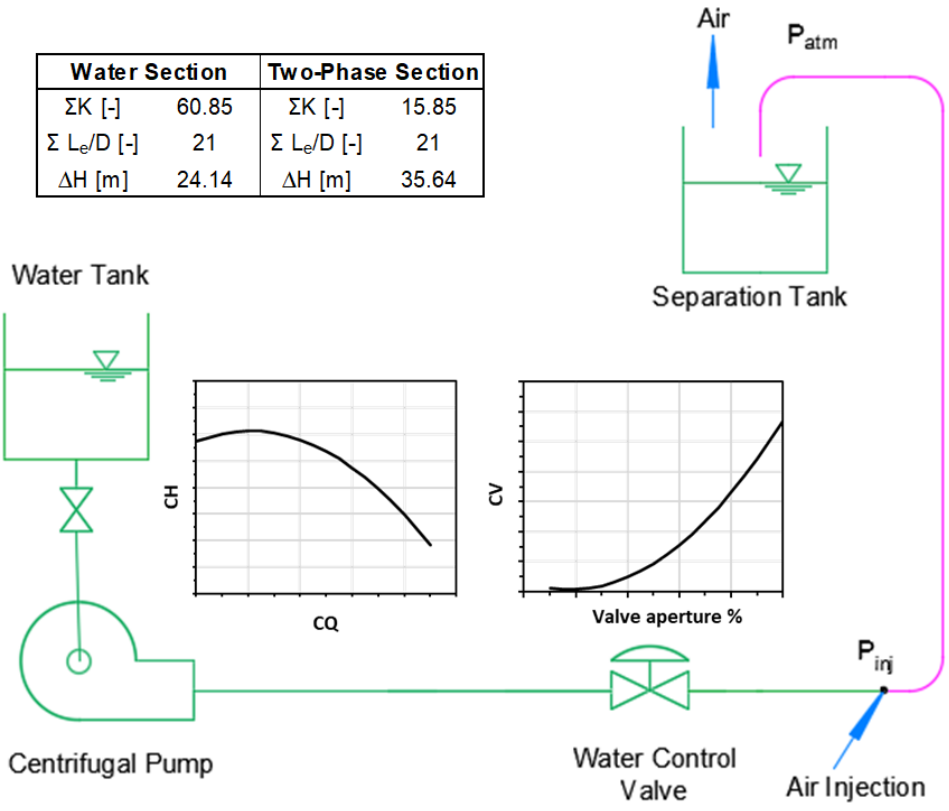

Figure 3. Simplified model of the experimental test section and the representation of the characteristic curves of the main components (pump and control valve); water section (—), air entrance (—), and two-phase section (—); the frame shows the total loss coefficient ($\sum K$), equivalent lengths ($\sum L_e/D$), and the height (ΔH) of the water and two-phase sections.

$$C_f = \begin{cases} \dfrac{16}{Re_M}, & laminar, \\ \dfrac{0.079}{Re_M^{0.25}}, & turbulent, \end{cases} \tag{5}$$

where Re_M is the Reynolds's number for the mixture and α is the void fraction. The drift relation first proposed by Zuber and Findlay (1965) can determine the void fraction in the mixture models, as shown in Eq. (6).

$$\frac{J_G}{\alpha} = C_0 J + C_\infty \sqrt{gD}, \tag{6}$$

where J_G is the superficial velocity of the gas phase, C_0 is the distribution parameter, and C_∞ is the drift coefficient. There are correlations for predicting the distribution parameter and the drift coefficient. Nonetheless, in the homogeneous case, the drift coefficient is zero, and the distribution parameter equals the unit. Thus, the void fraction and volumetric fraction (β) are the same in this condition. Equation (7) gives the void fraction for the homogeneous model:

$$\alpha = \beta = \frac{J_G}{J}. \tag{7}$$

Nonetheless, the gas's superficial velocity changes along the vertical line due to the gas expansion. Determining the injection pressure for the inputted gas superficial velocity at the atmospheric condition can result in an undersized system flow coefficient curve. Therefore, we must evaluate an average gas superficial velocity along the test section. We use an iterative calculation starting with the gas's superficial velocity at the atmospheric condition, one of the input parameters. Using this value, we determine the gas density using the open-source properties' library CoolProp and the injection pressure. Then, we calculate the gas superficial velocity at this injection pressure. This iterative calculus is made until the error between the previous and current steps is less than 0.1%. When this condition is achieved, the average J_G is calculated using the average values from the last two steps. Figure 4 shows this calculation procedure, where J_G^i is the initial gas superficial velocity at the atmospheric condition.

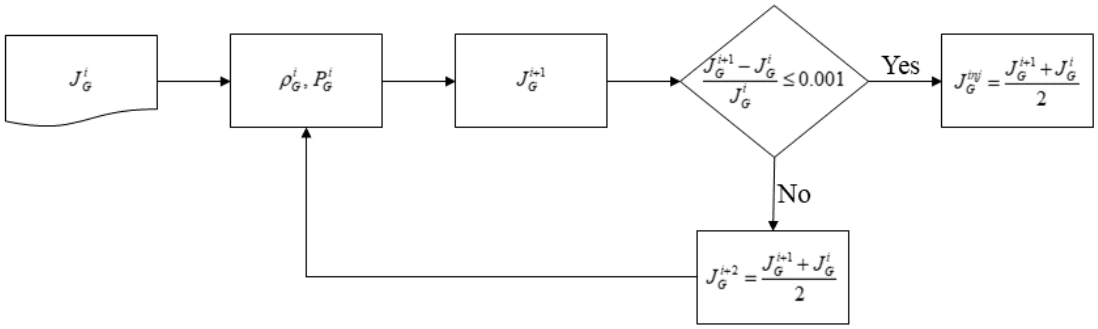

Figure 4. Flowchart of the procedure of calculating the average gas superficial velocity (J_G).

Additionally, we can estimate the pump head curve using Eq. (8) with the average superficial velocity of the gas phase and the injection pressure. This equation corresponds to the solid line part presented in Fig. 3.

$$H = \left[P_{inj} + g(\rho_L H_2 - \rho_L H_1) + \left(f\frac{L_e}{D} + K + K_{CV} \right) \frac{\rho_L J_L^2}{2} \right] \frac{1}{g\rho_L}, \tag{8}$$

where the terms L_e/D and K are the localized pressure drop along the line, and K_{CV} is the localized pressure drop at the control valve. Table 2 describes these minor head loss elements. H_1 is the liquid column height at the suction, and H_2 is the liquid column height at the discharge until the injection point. In this case, Darcy's friction factor can be estimated using the correlation of Swamee and Jain (1976), presented in Eq. (9).

$$f = \left[\left(\frac{64}{Re} \right)^8 + 9.5 \left[\ln\left(\frac{\epsilon/D}{3.7} + \frac{5.74}{Re^{0.9}} \right) - \left(\frac{2500}{Re} \right)^6 \right]^{-16} \right]^{\frac{1}{8}}. \tag{9}$$

Therefore, the flow conditions and the pump head curve determine the pump rotation for each control valve opening, which is contemplated in the K_{CV} term. The control valve opening is defined according to the pump's operational condition.

4. RESULTS AND DISCUSSION

The two main components in the single-phase part of the experimental setup for a control system are the water pump and the control valve. These two components have the nominal curves provided by the manufacturers; however, these curves are defined in a specific condition adopted by the manufacturer, which differs from our experimental condition. To encompass this difference, we performed an extensive experimental single-phase campaign to obtain the pump head curve CH and the valve flow coefficient CV. We fitted the nominal curves for both components with this experimental single-phase database. Figures 5(a) and 5(b) show the database and these fittings for pump head and valve flow coefficient curves, respectively.

In addition, we need to validate the model proposed to know if it agrees with the experimental data. Therefore, we performed a two-phase flow experimental campaign. The test grid was determined by varying the gas mass flow rate from 1.0 to 3.0 kg/h and liquid superficial velocity from 0.5 to 2.0 m/s, totaling 35 experimental points. We measured the absolute injection pressure for these points and compared it with the model predictions, as shown in Fig. 6. The numerical model could predict the pressure at the injection with less than 15% deviation for all data points, indicating a good agreement with experimental data.

The model proposed is based on the homogeneous model; however, it considers an average value of J_G and allows the prediction of the injection pressure, which is the critical value for controlling the system. Nonetheless, we can compare this model proposed with the homogeneous model in its classic form and with a drift-flux model using a similar approach as presented in Santim *et al.* (2020). The main advantage of these two last approaches is that they can also predict the pressure and gas superficial velocity along the line. In contrast, the model proposed can predict these parameters only at the injection point. In addition, the drift-flux model can achieve better results because the model takes into account the flow pattern. Therefore, we compared the three models for three experimental points (Tab. 3).

Figure 7 compares the numerical models' predictions using the drift-flux, homogeneous, and the proposed models with experimental data. As expected, the drift-flux model showed the best results of all models considered, presenting less than 8% deviation for pressure and less than 5% in predicting the superficial velocity of gas for all cases. In contrast, the

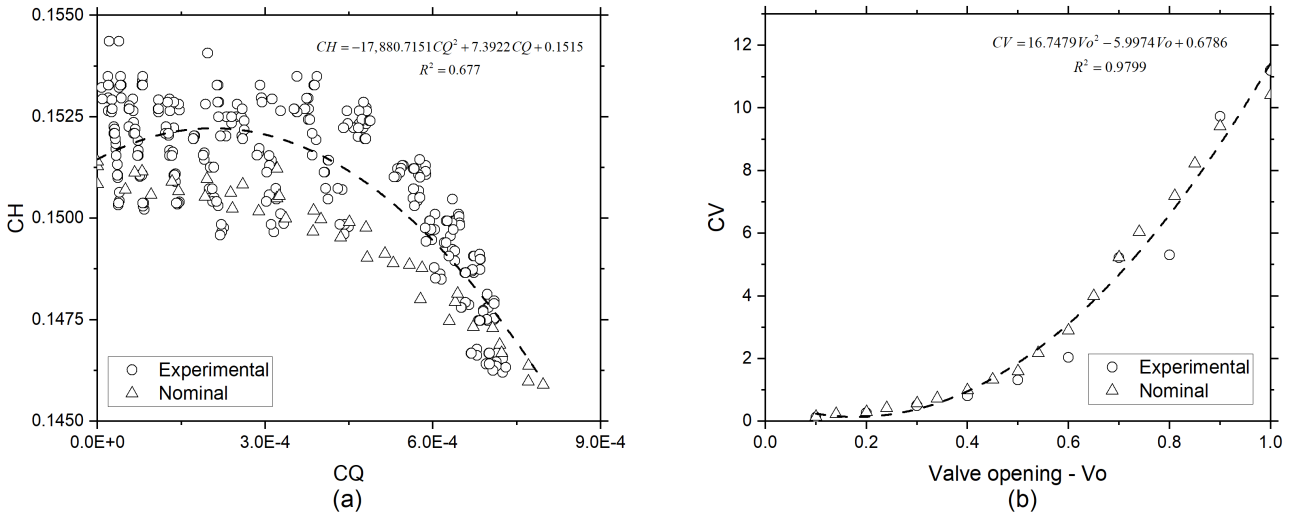

Figure 5. Curves fittings of the single-phase database and the nominal curves.

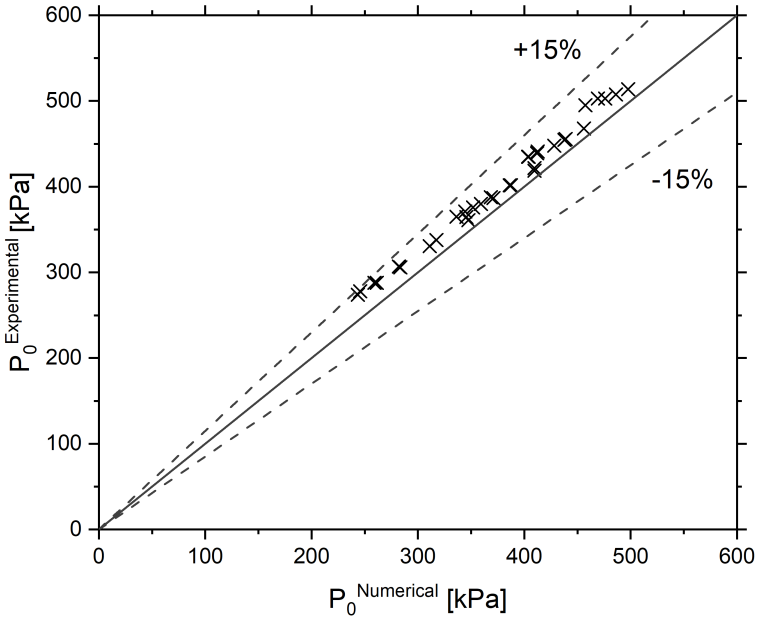

Figure 6. Comparison of numerical and experimental pressure at station S0.

Table 3. Test grid for model comparison.

Test #	$\dot{m}_G$ **[kg/h]**	J_L **[m/s]**
A	1.5	0.5
B	2.5	0.5
C	3.0	0.5

homogeneous model in its classical form presented the most significant deviation, being less than 30% for both pressure and gas velocity. Nonetheless, the proposed model performed better than the homogeneous model in predicting the flow variables at the injection point with less than 15% deviation.

For these points, the expected patterns along the 'S' curve of the lazy-wave riser are shown in Fig. 8 for points A, B, and C predicted by the drift-flux model. The slug pattern is observed in almost all stations, except in the downward part, where it transitioned to stratified flow. In any case, these patterns are out of the validity range of the homogeneous model.

Although the drift-flux model presented better results, the main limitation of this model is the computational time of the simulations because it needs an interactive method to solve the flow. This simulation time is crucial for controlling applications. They took 4, 5, and 6 minutes to run for Tests A, B, and C, respectively, using a computer with the configurations described in Tab. 4. Therefore, using the drift-flux model could compromise the operational agility of the controlling system. Another limitation of the drift-flux model is that the superficial velocities are input parameters; however, these

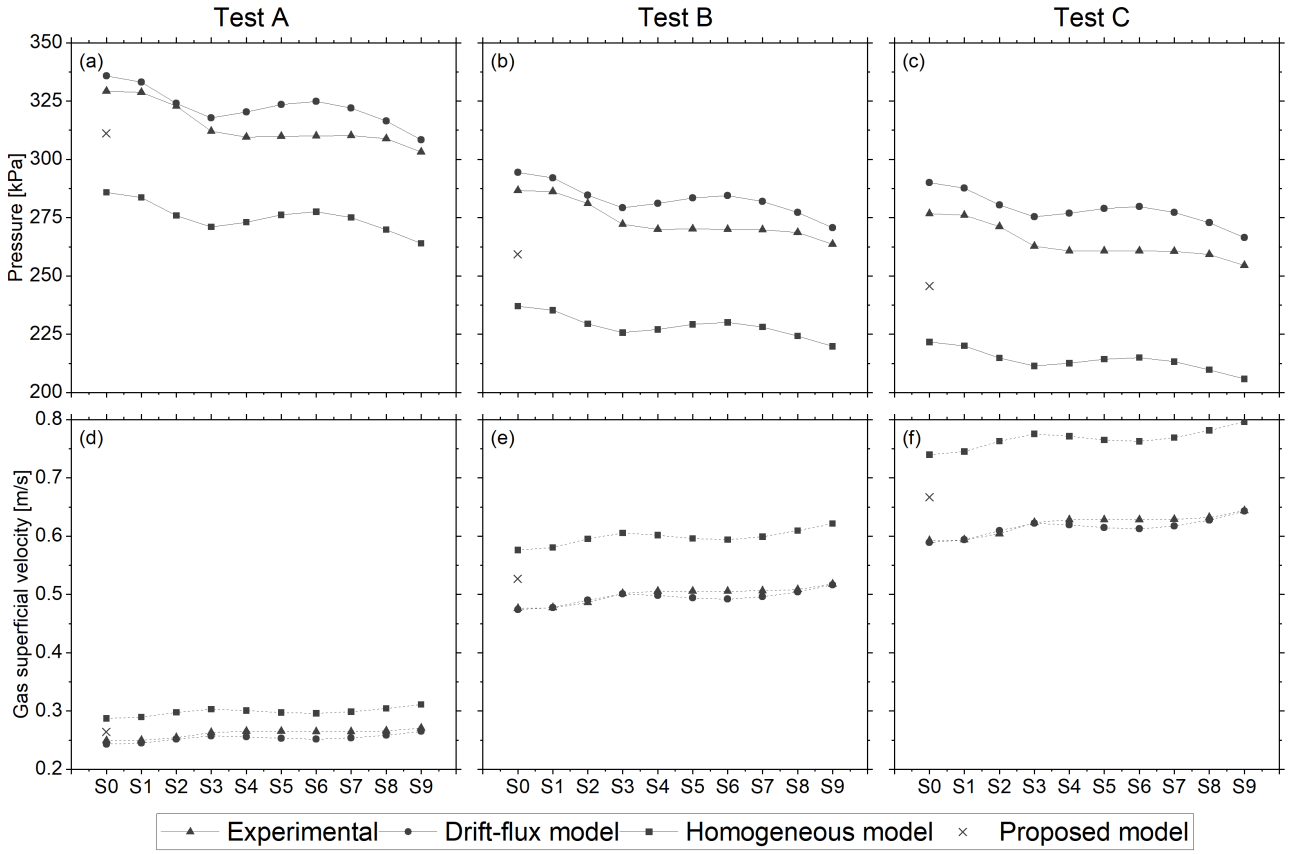

Figure 7. Comparison numerical models prediction and experimental data along the lazy-wave length. Graphs (a), (b), and (c) show the pressure, and graphs (d), (e), and (f) show the superficial gas velocity from the injection point (S0) to station nine (S9).

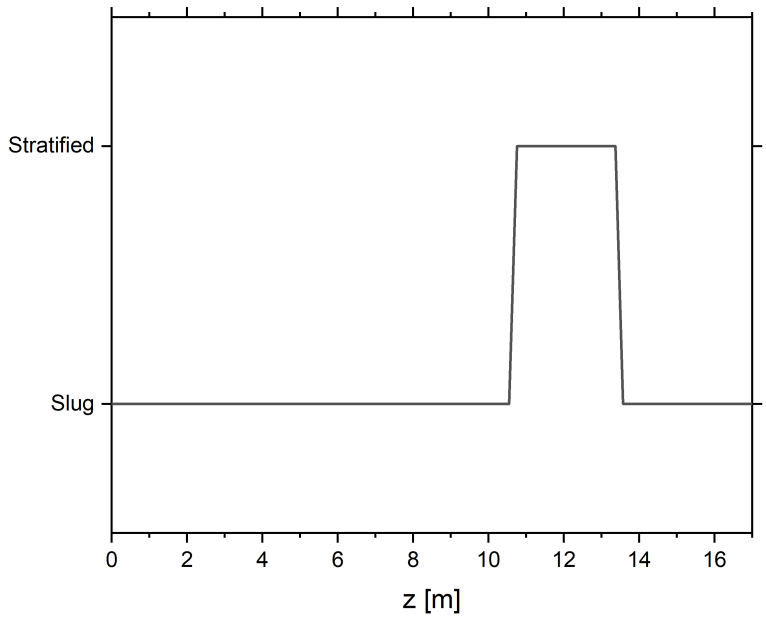

Figure 8. Flow patterns along the 'S' curve of the lazy-wave.

velocities are unknown without performing experimental runs.

We also performed an experimental two-phase flow campaign to verify the model capacity in predicting the pump rotation and the valve opening. Thus, we inputted the supervisory system with the numerical results of pump rotation and valve opening to obtain the desired liquid superficial velocity. We have guaranteed the gas superficial velocity control for all tests. Therefore, this method focuses only on liquid velocity control. Table 5 shows the test grid for this method

Table 4. Configuration of the computer used to simulate the flow employing the drift-flux model.

Itens	**Configuration**
Processor	Intel Core i9-7980XE 2.6 GHz
RAM memory	128 Gb
Hard drive	8 Tb
Operational system	Microsoft Windows 10 Pro (64 bits)
Video card	NVIDIA GeForce GTX 1050

validation. We chose these points to test the limits of our model within the test grid used in the pressure at S0 comparison; thus, for a similar mass flow rate of gas, the superficial liquid velocity was 0.5 and 2.0 m/s. In addition, an outlier point (Test #9) was tested to verify the model capacity. This point corresponds to a mass flow rate of gas of 3.865 kg/h and a liquid superficial velocity of 1.0 m/s.

Table 5. Test grid for method validation.

Test #	$\dot{\mathbf{m}}_G$ **[kg/h]**	J_G^{atm} **[m/s]**	J_L **[m/s]**	$\frac{J_G^{atm}}{J_L}$
1	1.55	0.896	0.5	1.792
2	1.42	0.821	2.0	0.411
3	2.00	1.159	0.5	2.319
4	2.06	1.193	2.0	0.596
5	2.48	1.436	0.5	2.873
6	2.54	1.469	2.0	0.735
7	2.59	1.502	0.5	3.003
8	2.95	1.701	2.0	0.851
9	6.82	3.865	1.0	3.865

Figure 9 compares the desired and the obtained values for the liquid superficial velocity. Our test grid has a ratio of superficial velocities from 0.4 to 3.9. We obtained a maximum of 20% deviation for all test points. As expected, the cases with the most significant deviation were the ones with the biggest ratio of superficial velocities. A solution for these cases with higher superficial velocity ratios is improving the mathematical model to predict the injection pressure using a drift-flux model, for example. Installing a pressure transducer at the injection point and using this pressure as indicated in the simplified model (Fig. 3) can also improve the controlling system; however, we continue depending on the initial set-point, which the model determines. Nonetheless, given the simplicity of the proposed model, it presented a good agreement with the experimental data.

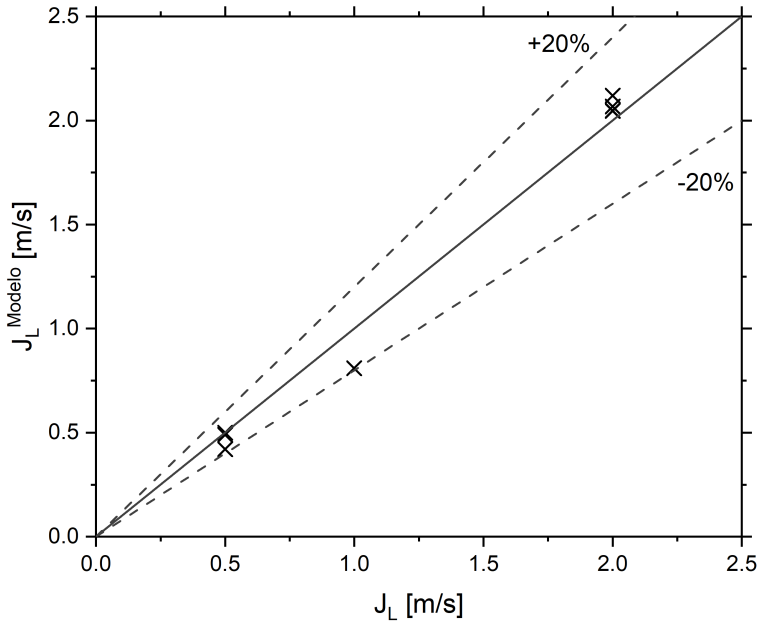

Figure 9. Comparison of the expected liquid superficial velocity and the value obtained by the model.

5. CONCLUSION

This paper presented a model for improving the control of liquid injection based on the homogeneous model. In addition, extensive experimental databases of single- and two-phase flows were used. The model was tested in a lazy-wave riser experimental apparatus scaled by a real riser from pre-salt. The model presented less than 15% deviation for predicting the pressure at the injection for all cases and less than 20% deviation in determining the liquid superficial velocity. Given the proposed model's simplicity and fast simulation time, it presented good results even for the biggest superficial velocity ratio. Therefore, using this model in a controlling system can deliver promising results. For future work, we aim to use this model in a controller based on artificial intelligence and implement this controller in our supervisory system. In addition, we also aim to explore the drift-flux model for controlling applications.

6. ACKNOWLEDGEMENTS

The authors acknowledge the financial support from PETROBRAS/FUNCAMP under contracts 5302, 5303, and 5512.

7. REFERENCES

Bahrami, B., Mohsenpour, S., Noghabi, H.R.S., Hemmati, N. and Tabzar, A., 2019. "Estimation of flow rates of individual phases in an oil-gas-water multiphase flow system using neural network approach and pressure signal analysis". *Flow Measurement and Instrumentation*, Vol. 66, pp. 28–36.

Bertola, V., 2014. *Modelling and experimentation in two-phase flow*, Vol. 450. Springer.

Ferraz, R., Mello, T., Borges Filho, M., Borges, R., Magalhães Filho, S., Scheid, C., Meleiro, L. and Calçada, L., 2022. "An experimental and theoretical approach on real-time control and monitoring of the apparent viscosity by fuzzy-based control". *Journal of Petroleum Science and Engineering*, Vol. 217, p. 110896.

Kanizawa, F.T. and Ribatski, G., 2021. *Flow boiling and condensation in microscale channels*. Springer.

Malhotra, R. and Sodhi, R., 2011. "Boiler flow control using pid and fuzzy logic controller". *IJCSET*, Vol. 1, No. 6, pp. 315–319.

Santim, C., Fulchignoni, L., Rosa, E. and Gaspari, E., 2020. "Transient multiphase flow modeling and validation in a real production system with high co2 content using the drift-flux model". *Journal of Petroleum Science and Engineering*, Vol. 188, p. 106903.

Shoham, O., 2006. "Mechanistic modeling of gas-liquid two-phase flow in pipes".

Swamee, P.K. and Jain, A.K., 1976. "Explicit equations for pipe-flow problems". *Journal of the hydraulics division*, Vol. 102, No. 5, pp. 657–664.

Wajman, R., 2019. "Computer methods for non-invasive measurement and control of two-phase flows: A review study". *Information technology and control*, Vol. 48, No. 3, pp. 464–486.

Wallis, G.B., 2020. *One-dimensional two-phase flow*. Courier Dover Publications.

Wang, H., Zhang, M. and Yang, Y., 2020. "Machine learning for multiphase flowrate estimation with time series sensing data". *Measurement: Sensors*, Vol. 10, p. 100025.

Yan, Y., Wang, L., Wang, T., Wang, X., Hu, Y. and Duan, Q., 2018. "Application of soft computing techniques to multiphase flow measurement: A review". *Flow Measurement and Instrumentation*, Vol. 60, pp. 30–43.

Zuber, N. and Findlay, J.A., 1965. "Average volumetric concentration in two-phase flow systems".

8. RESPONSIBILITY NOTICE

The authors are solely responsible for the information included in this paper.